Structure-Based Design of an Indolicidin Peptide Analogue with Increased Protease Stability[†,‡]

Annett Rozek,[§] Jon-Paul S. Powers, Carol L. Friedrich, and Robert E. W. Hancock*

Department of Microbiology and Immunology, University of British Columbia, #300-6174 University Boulevard, Vancouver, British Columbia, V6T 1Z3, Canada

Received September 11, 2003

ABSTRACT: Indolicidin is an antimicrobial cationic peptide with broad-spectrum activity isolated from bovine neutrophils. An indolicidin analogue CP-11, ILKKWPWWPWRRK-NH_2, with improved activity against Gram-negative bacteria had increased positive charge and amphipathicity while maintaining the short length of the parent molecule. The structure of CP-11 in the presence of dodecylphosphocholine (DPC) micelles was determined using nuclear magnetic resonance spectroscopy. CP-11 was found to be an amphipathic molecule with a U-shaped backbone bringing the N- and C-termini in close proximity. On the basis of this close proximity, a cyclic disulfide-bonded peptide cycloCP-11, ICLKKWPWWPWRRCK-NH_2, was designed to stabilize the lipid-bound structure and to increase protease resistance. The three-dimensional structure of cycloCP-11 was determined under the same conditions as for the linear peptide and was found to be similar to CP-11. Both CP-11 and cycloCP-11 associated with phospholipid membranes in a similar manner as indicated by circular dichroism and fluorescence spectra. The minimal inhibitory concentrations of CP-11 and cycloCP-11 for a range of bacteria differed by no more than 2-fold, and they were nonhemolytic at concentrations up to 256 μg/mL. Cyclization was found to greatly increase protease stability. The half-life of cycloCP-11 in the presence of trypsin was increased by 4.5-fold from 4 to 18 min. More importantly, the antibacterial activity of cycloCP-11, but not that of CP-11, in the presence of trypsin was completely retained up to 90 min since the major degradation product was equally active. A structural comparison of CP-11 and cycloCP-11 revealed that the higher trypsin resistance of cycloCP-11 may be due to the more compact packing of lysine and tryptophan side chains. These findings suggest that cyclization may serve as an important strategy in the rational design of antimicrobial peptides.

Cationic antimicrobial peptides play a key role in the immune system of many higher organisms such as plants, insects, amphibians, and mammals (*1*). On the basis of their rapid killing action, often within minutes of contact with microbes, cationic peptides have been suggested to constitute the first line of defense against invading bacteria, viruses, and fungi (*2*). With the alarming emergence of pathogens, which are resistant to conventional antibiotics, cationic peptides are being intensively studied with the objective of developing a novel class of antimicrobial drugs.

Indolicidin is a linear antimicrobial peptide isolated from the cytoplasmic granules of bovine neutrophils (*3*). The 13-amino acid sequence, ILPWKWPWWPWRR-NH_2, contains high fractions of tryptophan (39%) and proline and a unique, extended boat-shaped structure (*4*). Indolicidin has a broad spectrum of antimicrobial activity against Gram-positive and -negative bacteria (*3*), protozoa (*5*), fungi (*6*), and the enveloped virus HIV-1 (*7*). In addition, the peptide is cytotoxic to rat and human T-lymphocytes (*8*) and lyses erythrocytes (*6*). An indolicidin analogue CP-11, ILKKW-PWWPWRRK-NH_2, was designed to increase the number of positively charged residues, maintain the short length, and enhance amphipathicity, relative to indolicidin (*9*). CP-11 demonstrated improved activity against Gram-negative bacteria and *Candida albicans*, while it maintained the activity of indolicidin against staphylococci and showed reduced ability to lyse erythrocytes. In *Escherichia coli*, CP-11 was better able than indolicidin to permeabilize the outer membrane, as indicated by the enhanced uptake of 1-*N*-phenylnaphthylamine, and the inner membrane, as determined by the unmasking of cytoplasmic β-galactosidase.

The antimicrobial action of indolicidin is thought to involve interaction with the cytoplasmic membrane. We have recently determined the structure of native indolicidin in the presence of the membrane mimics dodecylphosphocholine (DPC)[1] and sodium dodecyl sulfate (SDS) micelles by nuclear magnetic resonance (NMR) spectroscopy (*4*). In the present paper, we have determined the three-dimensional structure of CP-11 in DPC to verify the structural require-

[†] We acknowledge funding from the Canadian Bacterial Diseases Network to R.E.W.H. R.E.W.H. is the recipient of a Canada Research Chair, while A.R. is the recipient of a Canadian Institutes of Health Research Postdoctoral Fellowship.

[‡] The structures of CP-11 and cycloCP-11 have been deposited at the PDB (http://www.rcsb.org/pdb/) as accession codes 1QXQ and 1QX9, respectively. The proton chemical shifts of CP-11 and cycloCP-11 have been deposited at the BMRB (http://www.bmrb.wisc.edu/) as accession codes BMRB-5938 and BMRB-5941, respectively.

* Corresponding author. Phone: (604) 822-2682. Fax: (604) 822-6041. E-mail: bob@cmdr.ubc.ca.

[§] Present address: Inimex Pharmaceuticals Inc., 6660 NW Marine Dr., Vancouver, GC, V6T 1X2, Canada.

10.1021/bi035643g CCC: $25.00 © 2003 American Chemical Society
Published on Web 11/11/2003

ments for the improved antimicrobial activity relative to indolicidin. Indeed, the amphipathicity of CP-11 was increased while the overall length of the molecule was reduced as compared to the parent peptide. The U-shaped peptide backbone brought the N- and C-termini of CP-11 into close proximity. We therefore speculated that cyclization of the molecule would stabilize the overall lipid-bound structure. At the same time, cyclization may enhance protease stability by fixing the mobile ends of the molecule in space, thus making protease attack more difficult. This is an important consideration since proteases abound in the human body, especially trypsin-like proteases (*10*), and could potentially limit the effectiveness of antimicrobial peptides. Cyclization and its effects on structural stability and antimicrobial activity have been described previously for magainin 2 and melittin (*11*) and histatin 3 (*12*). An increase in protease resistance was observed for a cyclic derivative of indolicidin containing a fortuitous tryptophan−tryptophan cross-link (*13*). Cyclization of CP-11 was achieved by inserting, near the ends of the peptide, two cysteine residues that formed a disulfide bridge upon oxidation. The resulting peptide, ICLKKWPWWPWRRCK-NH_2, was designated cycloCP-11. Since the positively charged side chains of CP-11, which are critical for its antimicrobial function, are distributed toward both ends of the peptide, cyclization should help in protecting the antimicrobial activity of the cyclic peptide in the presence of the arginine and lysine specific protease trypsin. Indeed, proteolytic digestion of cycloCP-11 by trypsin showed slower fragmentation as compared to the parent peptide CP-11, and the antimicrobial activity of cycloCP-11 was less affected in the presence of trypsin. To identify the structural basis for the better protection of the cyclic peptide against trypsin digestion, the three-dimensional structure of cycloCP-11 was determined by NMR in the presence of DPC. A comparison of the structures of linear CP-11 and cycloCP-11 proved that the flexibility near the basic residues was reduced. The lysine residues near the N-terminal side of the peptide clustered tightly with leucine and tryptophan side chains, which explained why trypsin digestion took place preferentially at the C-terminal end.

MATERIALS AND METHODS

Peptide Synthesis. The peptides CP-11 (ILKKWPWWPWRRK-NH_2) and cycloCP-11 (ICLKKWPWWPWRRCK-NH_2) were synthesized by *N*-(9-fluorenyl)methoxy carbonyl (Fmoc) chemistry at the Nucleic Acid Protein Service (NAPS) unit at the University of British Columbia. The peptide purity was confirmed by HPLC and mass spectrometry. CycloCP-11 was oxidized by stirring 15 mg of peptide in 200 mL of Tris buffer (10 mM), pH 7.4, at room temperature for 48 h. The peptide was subsequently lyophilized and purified using a reversed phase 15RPC-3 column (Amersham Pharmacia Biotech, Piscataway, NJ) on a LKB FPLC system (Amersham Pharmacia Biotech, Piscataway, NJ). The formation of a disulfide linkage was confirmed by mass spectrometry (MW 2083.61, $[M + H]^+$ 2084.7).

NMR Spectroscopy. The samples of CP-11 and cycloCP-11 were prepared by adding a solution of perdeuterated DPC (Cambridge Isotope Laboratories Inc., Andover, MA) in 10 mM sodium phosphate buffer (pH 5), containing 10% D_2O (Cambridge Isotope Laboratories Inc., Andover, MA), to the lyophilized peptide to give concentrations of 2 mM CP-11 and 200 mM DPC-d_{38}. The pH was adjusted to 4.6 (uncorrected for the isotope effect). NMR spectra for CP-11 were recorded at 37 °C on a Bruker AMX 600 MHz spectrometer. Homonuclear TOCSY, NOESY, and DQF-COSY spectra were acquired. Water suppression was achieved using the WATERGATE technique (*14*, *15*) or by presaturation during the recycling delay (2−2.5 s). Spectra were collected with 512−800 data points in F1, 2048 data points F2, and 32−64 transients. TOCSY spectra were acquired using the MLEV-17 pulse sequence (*16*) at a spin-lock time of 80 ms. NOESY spectra were recorded at mixing times of 100 and 150 ms. For cycloCP-11 TOCSY (60 ms spin-lock time), DQF-COSY and NOESY (100 ms mixing time) were acquired on a Varian Inova 600 MHz spectrometer, operated by the Laboratory of Molecular Biophysics at the University of British Columbia, using similar parameters as were used for CP-11. All NMR data were processed with NMRPipe (*17*). Resolution enhancement was achieved by apodization of the free induction decay with shifted squared sine-bell window functions. The data were zero-filled to twice the size prior to Fourier transformation. Spectra were baseline corrected using a fifth order polynomial function. All chemical shifts were referenced to internal 4,4-dimethyl-4-silapentane-1 sulfonate (DSS).

NOE Data Analysis and Structure Calculation. All NMR spectra were analyzed using NMRVIEW v.4.0.5 (*18*). NOE cross-peaks were integrated in the NOESY spectra using a mixing time of 100 ms. The NOE volumes were converted to distances, which were calibrated using the average NOE volume of resolved geminal methylene proton cross-peaks. The H^N-H^α distances thus calculated ranged within the covalently restricted range (2.3−3.1 Å). Each distance was converted to a distance restraint by calculating upper and lower distance bounds using the equations suggested by Hyberts et al. (*19*). Pseudo-atom corrections were applied by adding 1 and 1.5 Å to the upper distance bound for unresolved methylene protons and methyl groups, respectively, and 1.0 Å to the upper bounds of tryptophan aromatic ring protons. Distance restraints involving resolved methylene protons were float corrected by adding 1.7 Å to the upper bound. Structures were calculated using the DGII (Accelrys Inc., San Diego, CA) and X-PLOR programs. A set of 20 structures was generated using the distance geometry and simulated annealing algorithms of DGII. The best structures having low NOE distance violations were refined using X-PLOR (*20*). Final structures were selected based on low NOE distance restraint violations and low total energies as determined by X-PLOR.

Liposome Preparation. A chloroform solution of POPC or POPG (Avanti Polar Lipids Inc., Alabaster, AL) or an equipolar mixture of both lipids was dried under a stream of N_2. Residual solvent was removed by desiccation under

[1] Abbreviations: CD, circular dichroism; DPC, dodecylphosphocholine; D_2O, deuterium oxide; MIC, minimal inhibitory concentration; MALDI-TOF MS, matrix-assisted laser desorption/ionization mass spectrometry; NMR, nuclear magnetic resonance; NOESY, nuclear Overhauser effect spectroscopy; NOE, nuclear Overhauser enhancement; TOCSY, total correlated spectroscopy; DQF-COSY, double quantum-filtered correlated spectroscopy; POPC, 1-palmitoyl-2-oleoyl-*sn*-glycero-3-phosphocholine; POPG, 1-palmitoyl-2-oleoyl-*sn*-glycero-3-phosphoglycerol; Tris, tris(hydroxyethyl) amino methane.

vacuum for 2 h. The resulting lipid film was rehydrated in 10 mM phosphate buffer (pH 7.0). The suspension was put through five cycles of freeze−thaw to produce multilamellar liposomes, followed by extrusion through 0.1 mm double-stacked Poretics filters (AMD Manufacturing Inc., Mississauga, ON, Canada) using an extruder device (Lipex Biomembranes, Vancouver, BC, Canada).

Circular Dichroism Spectroscopy. Circular Dichroism (CD) spectra were obtained using a J-810 spectropolarimeter (Japan Spectroscopic Company, Tokyo, Japan). Each spectrum (190−250 nm) was the average of 10 scans using a quartz cell of 1 mm path length at room temperature. The scanning speed was 50 nm/min at a step size of 0.1 nm, 2 s response time, and 1 nm bandwidth. All samples were 50 μM peptide in 10 mM Tris buffer (pH 7.4). The concentrations of lipid or detergent were 2 or 10 mM, respectively. Spectra were baseline corrected by subtracting a blank spectrum of a sample containing all components except the peptide. Ellipticities were converted to mean residue molar ellipticities [θ] in units of deg cm^2/dmol.

Fluorescence Spectroscopy. Fluorescence emission spectra were recorded on an LS 50B spectrofluorimeter (Perkin-Elmer, Canada, Ltd., Markham, ON, Canada). Measurements were performed between 300 and 450 nm at 1 nm increments using a 1 cm quartz cell at room temperature. The excitation wavelength was set to 280 nm with both the excitation and the emission slit widths set to 4 nm. Spectra were baseline corrected by subtracting blank spectra of the corresponding lipid or detergent solutions without peptide. The samples contained 2 μM peptide and 0.5 mM lipid or 10 mM detergent in 10 mM HEPES buffer (pH 7.2).

Proteolytic Digestion. Digestion of CP-11 and cycloCP-11 by trypsin (Sigma Chemical Co., St. Louis, MO) was carried out using 50 μg/mL peptide and 0.2 μg/mL trypsin in 100 mM Tris buffer, pH 7.6, at room temperature. The progress of peptide cleavage after several reaction times ranging from 5 min to 4 h was monitored chromatographically using a reversed phase 15RPC-3 column (Amersham Pharmacia Biotech, Piscataway, NJ) on a LKB FPLC system (Amersham Pharmacia Biotech, Piscataway, NJ). The identity of digestion fragments was determined using mass spectrometry (MALDI-TOF) performed by the Nucleic Acid Protein Services (NAPS) unit at the University of British Columbia. The structure of the major fragment of cycloCP-11, which was ambiguous from molecular weight alone, was verified by cleaving the disulfide bond with dithiothreitol and identifying the resulting fragments by mass spectrometry (MALDI-TOF).

Protease Effects on Antimicrobial Activity. CP-11 and cycloCP-11 were incubated at 37 °C in the presence of trypsin at a peptide-to-trypsin ratio of 256:1 in 100 mM Tris buffer, pH 7.3. Peptide concentrations used for *S. epidermidis* and *E. coli* assays were 8 and 16 μg/mL, respectively. After the incubation period, *S. epidermidis* or *E. coli* cells, collected in mid-log phase, were added and incubated for 5 min. Aliquots of each sample were then diluted in Mueller−Hinton broth and incubated overnight on Mueller−Hinton agar, and the number of colony forming units was determined. Percent killing was calculated relative to the number of colony forming units from a sample incubated in the presence of trypsin alone.

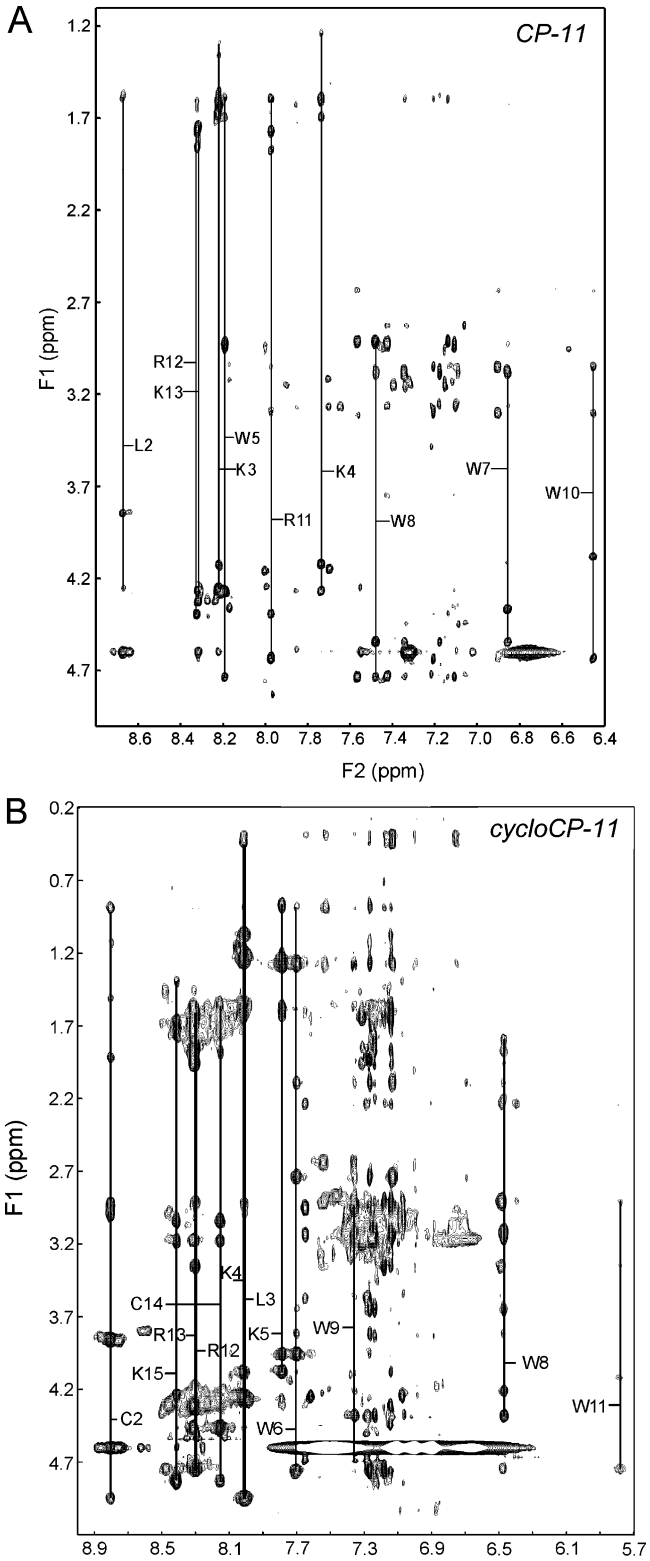

FIGURE 1: Fingerprint region of the two-dimensional ^{1}H NOESY spectra (τ_m 100 ms) of (A) CP-11 (2 mM) and (B) cycloCP-11 solubilized in DPC-d_{38} (200 mM) micelles at pH 4.6 and 37 °C. Amino acid spin systems are indicated by vertical lines and labels.

Minimal Inhibitory Concentration. The minimal inhibitory concentration of peptides was determined in triplicate using the modified broth microdilution assay (*21*). Serial dilutions of the peptide were made in Mueller−Hinton broth in 96-well polypropylene microtiter plates (Costar, Corning Inc., Corning, NY). Each well was inoculated with 10 μL of the test organism in Mueller−Hinton broth to a final concentra-

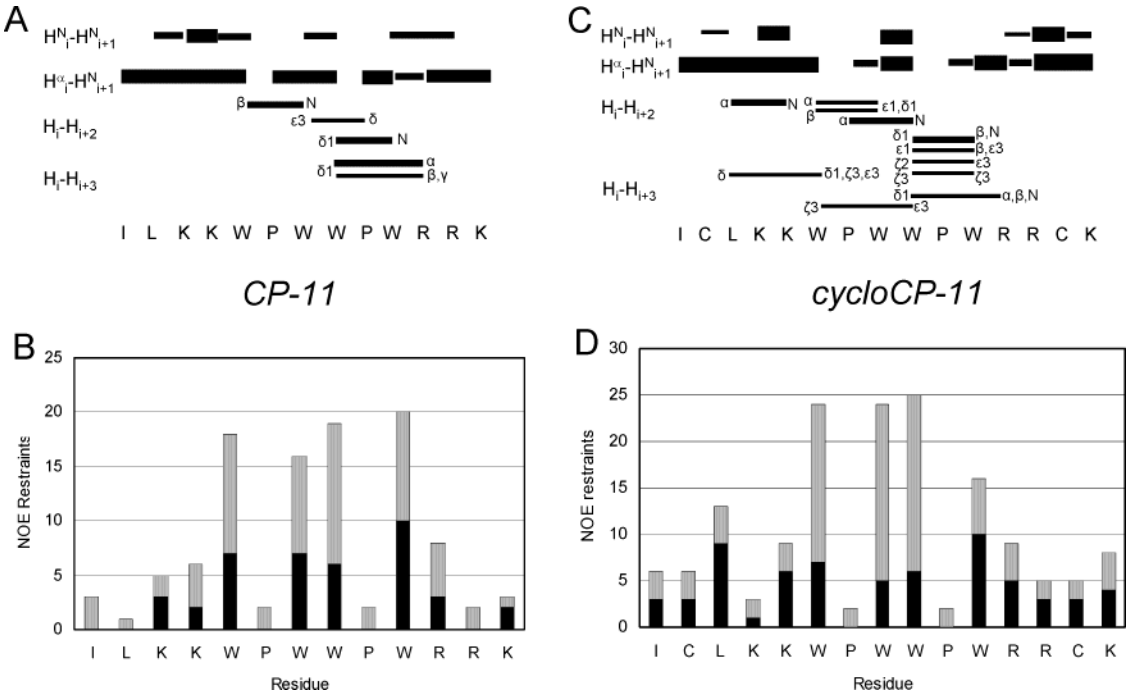

FIGURE 2: Distribution of NOE-based distance restraints observed for CP-11 and cycloCP-11. (A) Sequential and medium range NOE restraints of CP-11. The thickness of the bars corresponds to strong, medium, and weak contacts. (B) Number of intraresidue (black columns) and interresidue (gray columns) NOE restraints of CP-11. (C) Sequential and medium range NOE restraints of cycloCP-11. (D) Number of intraresidue and interresidue NOE restraints of cycloCP-11.

tion of approximately 10^5 cfu/mL. The MIC was taken as the lowest peptide concentration at which growth was inhibited by at least 50% after 24 h incubation at 37 °C. In experiments using trypsin, the peptide-to-trypsin ratio was kept at 256:1; the highest trypsin concentration was 1 μg/mL. Controls, testing only peptide or only trypsin, were run simultaneously.

Hemolytic Activity. Hemolytic activity of the peptides was tested against human red blood cells using slight modifications to the previously described method (*21*). Plates were incubated at 37 °C for 1 h with constant rocking. The degree of agglutination was determined by eye for each peptide concentration. Supernatant was collected from each well, and the absorbance was recorded at 540 nm using a Power Wave X 340 plate reader (Bio-Tek Instruments Inc., Winooski, VT). The assay was repeated in triplicate, and the average values were calculated. Percent lysis for each peptide concentration was calculated relative to a sample containing 1% Triton X-100, which was taken as 100%.

RESULTS

NMR Spectroscopy and Structures of CP-11 and cycloCP-11. The structures of CP-11 and cycloCP-11 were determined in the presence of DPC micelles (molar peptide to DPC ratio 1:100) using conventional solution NMR methods (*22*). Proton resonance assignments at 37 °C, pH 4.6, were made using TOCSY, NOESY, and DQF-COSY spectra. The fingerprint region of the NOESY spectra with spin system assignments is shown in Figure 1. Most NOE cross-peaks were well-resolved, and all sequential backbone cross-peaks were identified. The backbone amide proton resonances were spread over a wide range from 6.4 to 8.6 ppm for CP-11 and 5.7−8.9 ppm for cycloCP-11, which was due to the effects of tryptophan and proline on chemical shifts. Figure 2 summarizes the distribution, type, and strength of NOE contacts. A larger number of NOE cross-peaks was observed for cycloCP-11 than for CP-11. For CP-11, medium range NOE connectivities were observed mostly in the C-terminal half of the molecule, indicating the presence of secondary structure in this region. CycloCP-11 showed medium range restraints distributed throughout the sequence. The majority of NOE contacts involved the tryptophan side chains. The structures of CP-11 and cycloCP-11 were computed from a total of 105 and 157 nonredundant distance restraints, respectively, which were generated from the NOESY spectra recorded at 100 ms mixing time. Because of the high number of distance restraints involving the tryptophan residues, the central regions of both molecules were well-defined. A summary of the structural statistics is given in Table 1.

Table 1: Structural Statistics for the NMR-Derived Structures of CP-11 and CycloCP-11 in the Presence of DPC Micelles

	CP-11	cycloCP-11
no. of NOEs	105	157
intraresidue (nonredundant)	40	65
interresidue	65	92
no.[a] of NOE violations >0.1 Å	4 ± 1	16 ± 2
largest NOE violation (Å)[a]	0.18 ± 0.06	0.30 ± 0.11
final energies[a] (kcal/mol)[b]	30 ± 2	46 ± 3
RMSD bond length[c] (Å)	0.017	0.017
RMSD bond angles[c] (deg)	2.5	2.5
RMSD[d] (Å) backbone	0.26 ± 0.13 residues 5−11	0.42 ± 0.26 residues 2−11
RMSD[d] (Å) heavy	0.87 ± 0.22 residues 5−11	0.72 ± 0.24 residues 2−11
percentage of dihedral angles in allowed regions of Ramachandran plot[d,e]	100	97.3

[a] Mean ± standard deviation. [b] Determined using X-PLOR v.3.851. [c] Root-mean-square deviation to the mean coordinates calculated using Molmol v.2K.2. [d] Determined with Procheck v.3.4.4. [e] Determined for 12 structures for CP-11 and 10 structures for cycloCP-11.

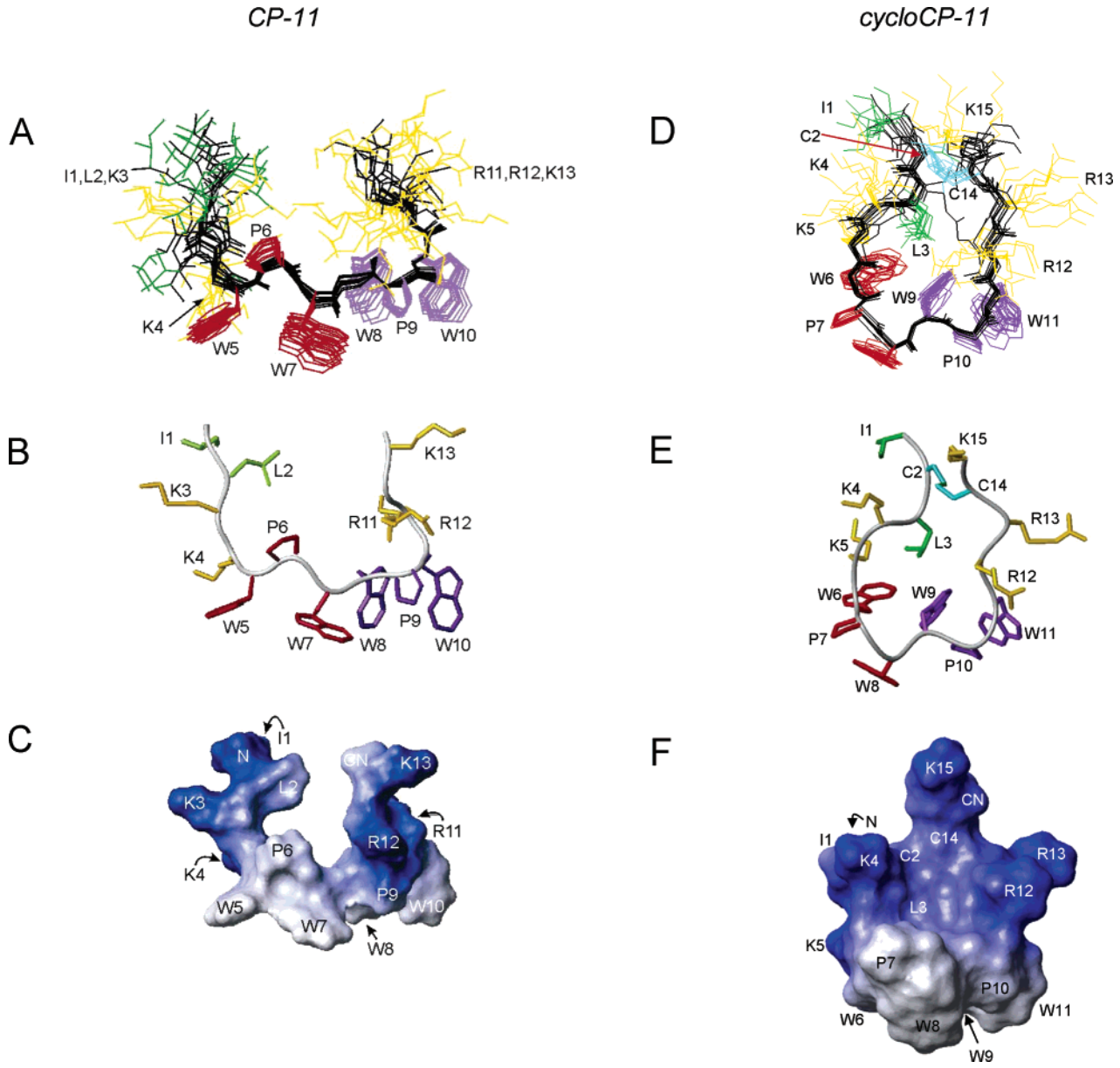

FIGURE 3: Calculated structures of CP-11 and ILKKWPWWPWRRK-NH_2 (A−C) and cycloCP-11 and ICLKKWPWWPWRRCK-NH_2 (D−F). (A) Set of 12 final structures for CP-11. Colors are green for Ile-1 and Leu-2, gold for basic amino acid side chains, and red and purple for the central tryptophan and proline side chains. (B) Model of CP-11 structure closest to the average illustrating the side chain orientation. The color-coding is the same as for panel A. (C) Contact surface of CP-11 painted with the electrostatic potential of the structure closest to the average. Blue represents positively charged and white represents uncharged regions. (D) Set of 10 final structures of cycloCP-11. (E) Model of cycloCP-11 structure closest to the average. (F) Contact surface of cycloCP-11. Coloring for cycloCP-11 illustrations corresponds to coloring for CP-11. This figure was prepared using the MOLMOL program (*38*).

The superposition of 12 final structures of CP-11 is shown in Figure 3A, while Figure 3B shows the structure closest to the average of 12 structures illustrating the side chain conformation. Because of the lack of NOE distance restraints, the N-terminal three and C-terminal two residues were disordered. The well-defined central region (residues 4−11) adopted an extended conformation dominated by two WPW motifs. Proline was predominantly in its trans-conformation as evidenced by strong NOE contacts between the δ-protons of proline and the α-protons of the preceding tryptophan residue. No NOE contacts between the α-protons of proline and the preceding tryptophan, indicative of the proline cis-conformation, were observed. In each WPW motif, the tryptophan residues faced the same side of the molecule, while the ring of the central proline pointed to the other side. The two WPW motifs were arranged in the opposite sense. While the central residues adopted dihedral angles typical of extended structure, two bends were centered at residues Lys-4 and Trp-10. These bends effected a reversal in backbone direction, bringing the N- and C-termini in relatively close contact (Figure 3B,C). Figure 3C shows the surface of CP-11 colored according to the electrostatic potential map. Positively charged regions (blue) were distributed toward both peptide termini, whereas hydrophobic areas (white) predominated in the central part of the molecule. The U-shaped curvature of the backbone positioned the positively charged residues mainly on one side of the molecule. With mostly hydrophobic proline and tryptophan residues on the other side, the structure of CP-11 was amphipathic.

On the basis of the relatively close spacing of the N- and C-terminal regions of CP-11, when bound to DPC, a cyclic derivative was designed. The structure of cycloCP-11, determined under the same conditions as were used for CP-11, is presented in Figure 3D−F. The structural ensemble shows a well-defined backbone structure including the terminal regions due to disulfide bond formation between Cys-2 and Cys-14. The backbone structure is highlighted by a type I turn between residues 6−9 (Trp-Pro-Trp-Trp). The average dihedral angles were $\varphi(i+1)$ −71°, $\psi(i+1)$ −4°, $\varphi(i+2)$ −121°, and $\psi(i+2)$ 44°, which was close to the ideal type I turn angles $\varphi(i+1)$ −60°, $\psi(i+1)$ −30°, $\varphi(i+2)$ −90°, and $\psi(i+2)$ 0° (*23*). The C═O···H—N distance between residues 6 and 9 was 2.75 Å, indicating a hydrogen bond. The residue Pro-7 is positioned at $(i+1)$ consistent with the high propensity of prolines for this position in type I turns (*24*). The type I turn was followed by a bend centered at Pro-10. Both turns were well-defined by several NOE restraints (Figure 2). A medium range NOE between Pro-7 H^{α} and Trp-9 H^{N} as well a strong NOEs between Trp-8 H^{N} and Trp-9 H^{N} were observed, which represent typical NOEs for type I turns (*25*). In addition, the residue Trp-6 showed several side chain interactions with Trp-8, while Trp-9 had multiple NOE contacts with Trp-11 and Arg-12. The aromatic rings of residues Trp-6, Trp-9, and Trp-11 nearly aligned on one side of the molecule at angles between 50 and 90° and intertryptophan distances of 5−6 Å. The side chain chemical shifts of residues Leu-3 and Lys-5 showed a significant high field shift (0.3−0.4 ppm) as compared to CP-11 due to aromatic ring current effects. This was accompanied by several NOE cross-peaks with Trp-6, which in the calculated structure resulted in a clustering of these side chains on the same molecular face as Trp-6, 9, and 11. Overall, the structure of cycloCP-11 is better defined and more compact than CP-11. The surface representation of cycloCP-11 (Figure 3F) shows an almost spherical molecule with an amphipathic charge distribution.

Fluorescence and CD of CP-11 and cycloCP-11. Figure 4 shows the fluorescence spectra of CP-11 and cycloCP-11. In aqueous buffer, CP-11 had an emission maximum at 356 nm, which shifted to lower wavelengths in the presence of lipid and increased in intensity. The blue shift was 6 nm for POPC, 8 nm for DPC, and 10 nm for POPG and mixed POPC:POPG vesicles. The blue shift of the emission maximum combined with an increase in quantum yield indicated that the tryptophan residues had moved to a less polar environment (*26*) upon association of the peptide with the lipid. CycloCP-11 had an emission maximum of 353 nm in aqueous buffer and a blue shift of 3 nm in POPC, 7 nm for DPC, 8 nm in POPC:POPG, and 10 nm in POPG vesicles.

The CD spectra of CP-11 and cycloCP-11 were recorded in aqueous buffer and in the presence of POPC and POPC:POPG large unilamellar vesicles as well as DPC micelles (Figure 5). The spectrum of both CP-11 and cycloCP-11 in aqueous buffer showed a broad negative band at 201 nm with intensities of −18 000 deg cm^2/dmol and −8400 deg cm^2/dmol, respectively. The position of this band has been assigned to unordered, β-turn, or polyproline II conformations (*4*, *27*, *28*). The strongly reduced intensity of this band in cycloCP-11 may have been due to a reduction of unordered conformation in the cyclic compound. The CD spectra in the presence of uncharged POPC liposomes were similar to the spectra in buffer, indicating that both peptides did not bind well to this lipid. This result was consistent with the small blue shift observed in the fluorescence spectra.

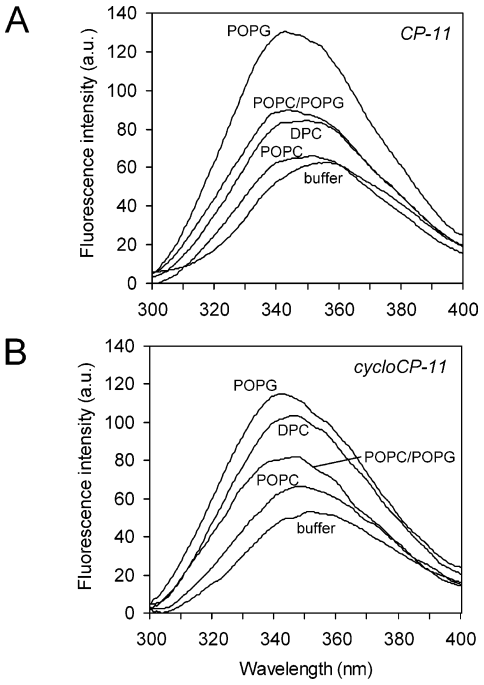

FIGURE 4: Fluorescence spectra of CP-11 (A) and cycloCP-11 (B) in aqueous solution and in the presence of DPC micelles and POPC, POPG, and POPC:POPG (1:1) large unilamellar vesicles. Samples contained 2 μM peptide in 10 mM HEPES buffer (pH 7.2) and 0.5 mM lipid or 10 mM DPC. Emission maxima for CP-11 are at 356 nm in buffer, 348 nm for DPC, 350 nm for POPC, and 346 nm for POPG and POPC:POPG (1:1). Emission maxima for cycloCP-11 are at 353 nm in buffer, 350 nm for POPC, 346 for DPC, 343 nm for POPG, and 345 nm for POPC:POPG (1:1).

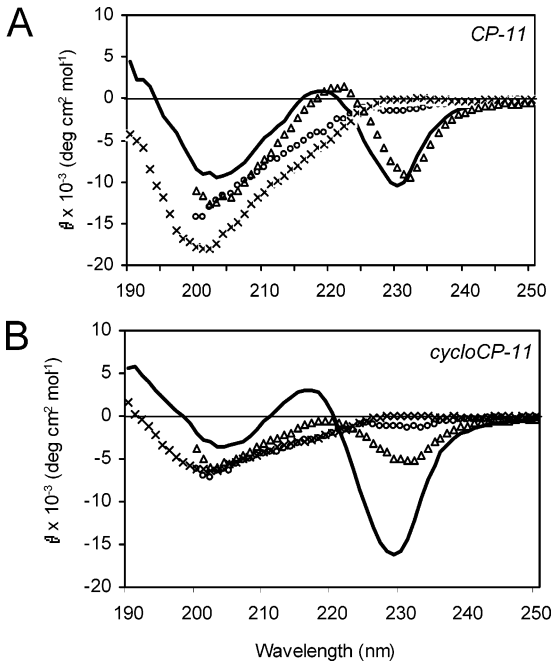

FIGURE 5: CD spectra of CP-11 (A) and cycloCP-11 (B) in aqueous buffer (×) and in the presence of DPC micelles (—), POPC (○), POPG (□), and POPC:POPG (1:1) (△) large unilamellar vesicles. Samples contained 50 μM peptide in 10 mM Tris buffer (pH 7.4) and 2 mM lipid or 10 mM DPC. Spectra of samples with lipid vesicles are not shown below 200 nm because of light scattering effects.

Table 2: Minimal Inhibitory Concentrations (μg/mL) of CP-11 and CycloCP-11 for Selected Gram-Negative and Gram-Positive Bacteria

bacterium	MIC (μg/mL)[a]	
	CP-11	CycloCP-11
E. coli wt	8	16
P. aeruginosa wt	16	64
S. typhimurium wt	64	64
S. typhimurium defensin sensitive	2	4
S. aureus wt	16	16
S. aureus methicillin resistant	16	16
S. epidermidis wt	4	8
E. faecalis wt	>64	64

[a] Data are representative of three determinations.

A significant change in the CD spectra was seen in the presence of negatively charged POPG and mixed POPC:POPG vesicles and DPC micelles. The negative band at 201 nm moved to ~205 nm and demonstrated reduced intensity with a more pronounced effect in the presence of POPG and DPC. Below 200 nm, a positive ellipticity was observed for CP-11 in DPC, but this was not observed in the presence of lipid vesicles due to light scattering (*29*). A second negative band appeared for both peptides at ~230 nm separated by a maximum at ~220 nm. The extensive changes to the CD spectra suggested an increase in secondary structure from a largely unordered conformation in aqueous buffer to a more ordered structure in the presence of negatively charged lipids. The strong contribution, to the CD spectra, of the four tryptophan residues in these peptides prevented the secondary structure estimation by common deconvolution methods. However, the second negative band at ~230 nm has been assigned to the tryptophan contribution, which depends on the orientation of the tryptophan aromatic ring relative to the peptide backbone (*30*). The CD spectrum of cycloCP-11 in DPC showed an especially large effect, which may be due to an additional contribution from an exciton couplet between tryptophan aromatic rings (*21*, *24*). Having the same types of maxima and minima, the CD spectra indicated that the secondary structures of CP-11 and cycloCP-11 were similar in mixed POPC:POPG and POPG lipid environments.

Antimicrobial and Hemolytic Activity of CP-11 and CycloCP-11. The minimal inhibitory concentrations (MIC) of CP-11 and its cyclic analogue were determined for several common Gram-negative and -positive bacteria (Table 2). CycloCP-11 exhibited a similar activity as compared to CP-11, the MICs being within 2-fold for most bacteria (considered the margin of error for this assay), except against *P. aeruginosa* for which the change was 4-fold. Linear CP-11 has previously been demonstrated to have low hemolytic activity in contrast to its parent molecule indolicidin that lyses erythrocytes at 32 μg/mL (*9*). Less than 5% hemolysis of human erythrocytes was observed after 1 h of treatment with CP-11 and cycloCP-11 at concentrations up to 256 μg/mL. Some red blood cell agglutination was seen with both peptides at concentrations higher than 32 μg/mL and was about twice as high for cycloCP-11 (50%) as for CP-11 (25%) at peptide concentrations of 64 μg/mL after 1 h of treatment.

Proteolytic Digestion of CP-11 and cycloCP-11. Figure 6A,B shows the chromatographic traces monitoring the degradation of CP-11 and cycloCP-11, respectively, by trypsin over time. At a peptide-to-trypsin ratio of 250:1, two fragments were generated from CP-11 at 9.6 min (peak 1) and one at 10.7 min retention time (peak 2). The fragments were identified by mass spectrometry (Table 3) as successive C-terminal truncation products (peaks 1 and 2) that would alter the charge from +6 to +3 and a core fragment (peak 2) with a charge of +2. For cycloCP-11, two fragments were detected at 9.2 min (peak A) and 10.7 min retention time (peak B). The digestion proceeded much slower for cycloCP-11 than for CP-11, producing mainly one fragment after 60 min (peak A) that was identified as the Arg-13 cleavage

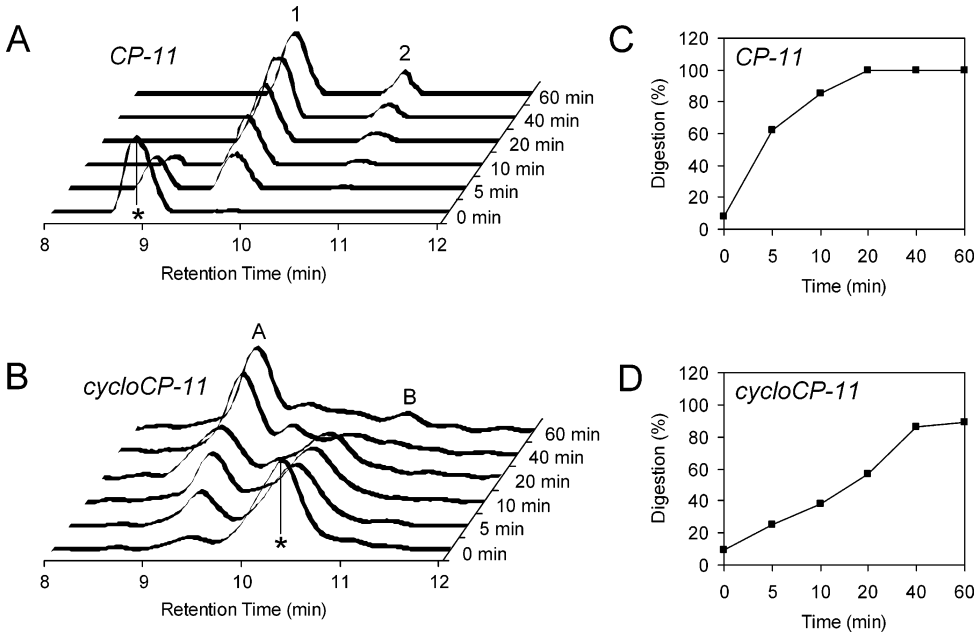

FIGURE 6: Proteolytic digestion of CP-11 and cycloCP-11 by trypsin. (A and B) HPLC traces of CP-11 (A) and cycloCP-11 (B) after different reaction times (listed is the starting time of the chromatographic run). Peak detection was by absorbance at 280 nm. The molecular peak is indicated by an asterisk. (C and D) Degradation of CP-11 (C) and cycloCP-11 (D) estimated from the decrease of molecular peak area. Degradation is nonzero at time zero due to the delay of chromatographic separation caused by travel of the reaction mixture.

Table 3: Peptide Fragments of CP-11 and CycloCP-11 Generated by Trypsin Digestion after 60 min Reaction Time

	amino acid sequence	MW (g/mol)	$[M + H]^{+a}$
CP-11	ILKKWPWWPWRRK-NH_2	1879.32	n.d.[b]
peak 1 (71%)[c]	ILKKWPWWPWRR	1752.14	1753.2
peak 2 (29%)	ILKKWPWWPWR	1595.96	1597.3
	WPWWPWRR	1269.48	1270.5
cycloCP-11	ICLKKWPWWPWRRCK-NH_2	2083.61	n.d.
peak A[d] (67%)	ICLKKWPWWPWRR CK-NH_2	2101.61	2102.2
peak B (11%)	WPWWPWRR	1269.48	1270.2

[a] The molecular weight was determined by MALDI-TOF MS on the isolated HPLC fractions. [b] Not determined; there were no undigested peptides after 60 min reaction time. [c] Percentage of total peak area. [d] The identity of this fragment was verified by mass spectrometry of the purified fragment treated with dithiothreitol to cleave the disulfide bond. Only one cleavage product was observed corresponding to the sequence ICLKKWPWWPWRR (MW: 1855.30 g/mol, $[M + H]^+$: 1856.1).

product. This compound, due to an intact disulfide bond, retained the size and charge of the original peptide. The progress of digestion was estimated from the decrease of the molecular peak area of CP-11 and cycloCP-11 at 8.9 and 10.3 min retention time, respectively (Figure 6C,D). The half-life of cycloCP-11 in the presence of trypsin was increased by 4.5-fold from 4 to 18 min.

Protease Effects on Antimicrobial Activity. The protease effects on bacterial killing were determined by incubating each peptide with trypsin for a given amount of time followed by a 5 min incubation with the bacterial sample (Figure 7). The peptide concentrations used were 8 μg/mL for *S. epidermidis* and 16 μg/mL for *E. coli* corresponding to one times the MIC for cyloCP-11 and two times the MIC for CP-11. For both bacterial samples, cycloCP-11 caused 100% killing after 90 min incubation with trypsin. Conversely, killing by CP-11 began to decrease after 20 min (*S. epidermidis*) and 30 min (*E. coli*) of trypsin treatment and dropped below 50% killing after 90 min. The effects of protease treatment were more pronounced in the assay involving *S. epidermidis*, with CP-11 eliciting less than 20% killing after 90 min incubation with trypsin. This was also reflected by measurement of the MICs of CP-11 and cycloCP-11 against *S. epidermidis* in the absence and presence of trypsin. Against *S. epidermidis*, the activity of cycloCP-11 was not affected by trypsin treatment, whereas that of CP-11 was decreased 4-fold.

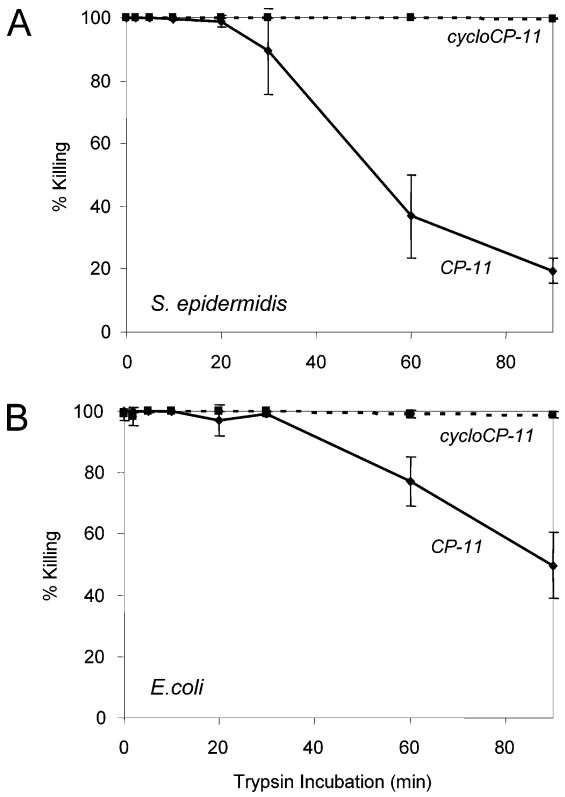

FIGURE 7: Protease effects on killing by CP-11 and cycloCP-11. Percent killing of *S. epidermidis* (A) and *E. coli* (B) by CP-11 (—) and cycloCP-11 (••••) after incubation with trypsin. Peptides were incubated with trypsin (peptide/trypsin = 256:1 w/w) for different reaction times at 37 °C. Bacterial cells collected in mid-log phase were added and incubated for 5 min, and the colony forming units were determined. Peptide concentrations were 8 μg/mL for *S. epidermidis* and 16 μg/mL for *E. coli.*

DISCUSSION

In this paper, we have analyzed the three-dimensional structure of the antimicrobial peptide CP-11, an indolicidin analogue that has improved activity against Gram-negative bacteria (*9*). The peptide CP-11 exerts its antimicrobial action after binding to the bacterial cytoplasmic membrane. Previous studies established that the improved activity of CP-11 as compared to indolicidin against Gram-negative species is associated with a better ability to permeabilize both the outer and the inner membrane (*9*). More recent studies using model membranes show that CP-11 inserts strongly into lipid monolayers but does not promote lipid flip-flop or vesicle leakage to a great extent, nor does it translocate across the bilayer of a liposome (*31*). Nevertheless, the activity against *E. coli* is dependent on the cytoplasmic membrane potential gradient (oriented internal negative), which could drive the peptide across the membrane in intact cells (*9*). In keeping with this, electron micrographs indicate that CP-11 is able to cause intracellular effects in Gram-positive bacteria, such as nuclear condensation and mesosome formation (*32*), as well as to inhibit macromolecular synthesis of DNA, RNA, and proteins (our unpublished data). Here, the interaction of CP-11 with model membranes and its effect on secondary structure was analyzed using fluorescence and CD spectroscopy. CP-11 bound preferentially to negatively charged vesicles, as demonstrated by the larger blue shift of the fluorescence maximum and the significant changes to the CD spectra in the presence of POPG and mixed POPC:POPG vesicles as compared to POPC vesicles. The deselection of neutral membranes as indicated by limited binding of CP-11 to POPC vesicles may be related to the reduced ability to lyse human erythrocytes. This effect has been observed for a number of cationic antimicrobial peptides and may be explained by an accumulation of positive charge (of the peptide molecules) on the surface of neutral vesicles, which leads to electrostatic repulsion and limited binding. However, CP-11 associated well with neutral DPC micelles, probably, since only a single peptide molecule became bound per micelle, and an accumulation of positive charge did not take place.

The conformation of CP-11 in DPC micelles, determined by NMR, was U-shaped with hydrophobic tryptophan and proline residues clustered on one side and positively charged

lysine and arginine residues clustered on the adjacent side of the molecule. Such an amphipathic amino acid distribution is common for antimicrobial peptides (*33*). A distinct feature of CP-11 and a few other antimicrobial peptide structures (*4*, *34*, *35*) is that it is rich in aromatic residues and proline, which leads to a backbone-fold that is different from the regular α-helical or β-sheet conformations. These structures combine extended and turn-like backbone geometries and are stabilized by few or no peptide backbone hydrogen bonds. The major stabilizing interaction appears to be between the peptide and the membrane, involving an important contribution of aromatic amino acids, and is of a complex electrostatic and hydrophobic nature (*36*, *37*).

A major limitation to the deployment of cationic peptide antibiotics as human therapeutics is the susceptibility of peptides to degradation by proteases in the body (*2*). Of great concern are trypsin-like proteases that abound in the body and are selective for basic residues. Because of the importance of positive charge for the antibiotic action of cationic peptides, the loss of the basic amino acids is critical. Furthermore, the basic amino acids are in the flexible part of the molecule and more vulnerable to protease attack than the more tightly packed hydrophobic residues. Thus, strategies that induce increased trypsin-like protease resistance are of great interest. We reasoned that constraining the backbone of an indolicidin-like peptide would be one such strategy. Therefore, based on the DPC-bound structure of CP-11, a cyclic analogue, cycloCP-11, was designed to possess higher protease resistance.

The proteolytic digestion by trypsin, monitored by HPLC, indicated a strongly reduced ability of the protease to degrade the cyclic peptide as compared to linear CP-11 with the half-life increasing by 4.5-fold from 4 to 18 min. These results explain the relative improvement of antimicrobial activity of cycloCP-11 cf. CP-11, in the presence of trypsin. Furthermore, the primary digestion product of cycloCP-11 had the same charge as its parent molecule, while that of CP-11 had a reduced positive charge. Indeed, as shown by mass spectrometry, digestion of cycloCP-11 resulted mainly in its linearization without any loss of amino acid residues. Since antibacterial activity was preserved after incubation with trypsin, we assume that this digestion product had antimicrobial activity at least equal to that of cycloCP-11.

Fluorescence and CD spectroscopy indicated that both linear CP-11 and cycloCP-11 formed similar interactions with phospholipids. The structure of cycloCP-11 in the presence of DPC, determined by NMR, showed that the cyclization of CP-11 maintained its amphipathic structure, while it led to a more rigid backbone and more compact packing of the side chains. This was particularly true for the cationic residues. The increased bulkiness likely reduced the interactions with trypsin through steric hindrance and slowed proteolysis. For both CP-11 and cycloCP-11, trypsin attack initiated at the C-terminal arginine, suggesting that the (near) N-terminal lysine residues were somewhat protected by interaction with nearby side chains. Indeed, the structure of cycloCP-11 showed a clustering of Lys-5, Trp-6, and Leu-3.

In this paper, we have demonstrated a structure-based approach to improving the potential utility of an antimicrobial peptide. Higher protease stability of peptides significantly extends the range of clinical applications and the cyclization of antimicrobial peptides by a disulfide bridge appears to be a simple strategy to accomplish this.

REFERENCES

1. Boman, H. G. (1995) *Annu. Rev. Immunol. 13*, 61−92.
2. Hancock, R. E. W. (2001) *Lancet. Infect. Dis. 1*, 156−64.
3. Selsted, M. E., Novotny, M. J., Morris, W. L., Tang, Y. Q., Smith, W., and Cullor, J. S. (1992) *J. Biol. Chem. 267*, 4292−5.
4. Rozek, A., Friedrich, C. L., and Hancock, R. E. W. (2000) *Biochemistry 39*, 15765−74.
5. Aley, S. B., Zimmerman, M., Hetsko, M., Selsted, M. E., and Gillin, F. D. (1994) *Infect. Immun. 62*, 5397−403.
6. Ahmad, I., Perkins, W. R., Lupan, D. M., Selsted, M. E., and Janoff, A. S. (1995) *Biochim. Biophys. Acta 1237*, 109−14.
7. Robinson, W. E., Jr., McDougall, B., Tran, D., and Selsted, M. E. (1998) *J. Leukocyte Biol. 63*, 94−100.
8. Schluesener, H. J., Radermacher, S., Melms, A., and Jung, S. (1993) *J. Neuroimmunol. 47*, 199−202.
9. Falla, T. J., and Hancock, R. E. W. (1997) *Antimicrob. Agents Chemother. 41*, 771−5.
10. Caughey, G. H. (1997) *Am. J. Respir. Cell Mol. Biol. 16*, 621−8.
11. Unger, T., Oren, Z., and Shai, Y. (2001) *Biochemistry 40*, 6388−97.
12. Brewer, D., and Lajoie, G. (2002) *Biochemistry 41*, 5526−36.
13. Osapay, K., Tran, D., Ladokhin, A. S., White, S. H., Henschen, A. H., and Selsted, M. E. (2000) *J. Biol. Chem. 275*, 12017−22.
14. Piotto, M., Saudek, V., and Sklenar, V. (1992) *J. Biomol. NMR 2*, 661−5.
15. Sklenar, V., Piotto, M., Leppik, R., and Saudek, V. (1993) *J. Magn. Reson. A102*, 241−5.
16. Bax, A., and Davis, D. G. (1985) *J. Magn. Reson. 65*, 355−60.
17. Delaglio, F., Grzesiek, S., Vuister, G. W., Zhu, G., Pfeifer, J., and Bax, A. (1995) *J. Biomol. NMR 6*, 277−93.
18. Johnson, B. A., and Blevins, R. A. (1994) *J. Biomol. NMR 4*, 603−14.
19. Hyberts, S. G., Goldberg, M. S., Havel, T. F., and Wagner, G. (1992) *Protein Sci. 1*, 736−51.
20. Nilges, M., Kuszewski, J., and Brunger, A. T. (1991) Computational aspects of the study of biological macromolecules by NMR, Plenum Press, New York.
21. Zhang, L., Benz, R., and Hancock, R. E. W. (1999) *Biochemistry 38*, 8102−11.
22. Wuthrich, K. (1986) *NMR of Proteins and Nucleic Acids*, Wiley, New York.
23. Venkatachalam, C. M. (1968) *Biopolymers 6*, 1425−36.
24. Hutchinson, E. G., and Thornton, J. M. (1994) *Protein Sci. 3*, 2207−16.
25. Wagner, G., Neuhaus, D., Worgotter, E., Vasak, M., Kagi, J. H., and Wuthrich, K. (1986) *J. Mol. Biol. 187*, 131−5.
26. Lakowicz, J. R. (1983) *Principles of fluorescence spectroscopy*, Plenum Press, New York.
27. Ladokhin, A. S., Selsted, M. E., and White, S. H. (1999) *Biochemistry 38*, 12313−9.
28. Falla, T. J., Karunaratne, D. N., and Hancock, R. E. W. (1996) *J. Biol. Chem. 271*, 19298−303.
29. Wallace, B. A., and Mao, D. (1984) *Anal. Biochem. 142*, 317−28.
30. Woody, R. W. (1994) *Eur. Biophys. J. 23*, 253−62.
31. Zhang, L., Rozek, A., and Hancock, R. E. W. (2001) *J. Biol. Chem. 276*, 35714−22.
32. Friedrich, C. L., Moyles, D., Beveridge, T. J., and Hancock, R. E. W. (2000) *Antimicrob. Agents Chemother. 44*, 2086−92.
33. Epand, R. M., and Vogel, H. J. (1999) *Biochim. Biophys. Acta 1462*, 11−28.
34. Schibli, D. J., Hwang, P. M., and Vogel, H. J. (1999) *Biochemistry 38*, 16749−55.
35. Tinoco, L. W., Da Silva, A., Jr., Leite, A., Valente, A. P., and Almeida, F. C. L. (2002) *J. Biol. Chem. 277*, 36351−6.
36. Ladokhin, A. S., and White, S. H. (2001) *J. Mol. Biol. 309*, 543−52.
37. Wimley, W. C., and White, S. H. (1996) *Nat. Struct. Biol. 3*, 842−8.
38. Koradi, R., Billeter, M., and Wuthrich, K. (1996) *J. Mol. Graph. 14*, 51−5, 29−32.

BI035643G